

**Weierstraß-Institut**  
**für Angewandte Analysis und Stochastik**  
**Leibniz-Institut im Forschungsverbund Berlin e. V.**

Preprint

ISSN 2198-5855

**Models and numerical methods for electrolyte flows**

Jürgen Fuhrmann, Clemens Gohlke, Alexander Linke, Christian Merdon, Rüdiger Müller

submitted: July 25, 2018

Weierstrass Institute  
Mohrenstr. 39  
10117 Berlin  
Germany  
E-Mail: [juergen.fuhrmann@wias-berlin.de](mailto:juergen.fuhrmann@wias-berlin.de)  
[clemens.gohlke@wias-berlin.de](mailto:clemens.gohlke@wias-berlin.de)  
[alexander.linke@wias-berlin.de](mailto:alexander.linke@wias-berlin.de)  
[christian.merdon@wias-berlin.de](mailto:christian.merdon@wias-berlin.de)  
[ruediger.mueller@wias-berlin.de](mailto:ruediger.mueller@wias-berlin.de)

No. 2525

Berlin 2018



---

2010 *Mathematics Subject Classification.* 35Q35, 35Q61, 78A57, 80A17.

*Key words and phrases.* Electro-thermodynamics, electroosmosis, ion transport, finite ion size, solvation.

This research has been supported by the German Federal Ministry of Education and Research Grant 03EK3027D (Network "Perspectives for Rechargeable Magnesium-Air batteries") and the Einstein Center of Mathematics, Berlin, project CH11 "Sensing with Nanopores".

Edited by  
Weierstraß-Institut für Angewandte Analysis und Stochastik (WIAS)  
Leibniz-Institut im Forschungsverbund Berlin e. V.  
Mohrenstraße 39  
10117 Berlin  
Germany

Fax: +49 30 20372-303  
E-Mail: [preprint@wias-berlin.de](mailto:preprint@wias-berlin.de)  
World Wide Web: <http://www.wias-berlin.de/>

# Models and numerical methods for electrolyte flows

Jürgen Fuhrmann, Clemens Gohlke, Alexander Linke, Christian Merdon, Rüdiger Müller

## Abstract

The most common mathematical models for electrolyte flows are based on the dilute solution assumption, leading to a coupled system of the Nernst-Planck-Poisson drift-diffusion equations for ion transport and the Stokes resp. Navier-Stokes equations for fluid flow. This contribution discusses historical and recent model developments beyond the dilute solution assumption and focuses on the effects of finite ion sizes and solvation. A novel numerical solution approach is presented and verified here which aims at preserving on the discrete level consistency with basic thermodynamic principles and structural properties like independence of flow velocities from gradient contributions to external forces.

## 1 Introduction

Liquid electrolytes are fluidic mixtures containing electrically charged ions. Electrochemical energy conversion systems like fuel cells and batteries contain liquid electrolytes. In biological tissues, nanoscale pores in the cell membranes separate different types of ions inside the cell from those in the intercellular space. Nanopores between electrolyte reservoirs can be used for analytical applications in medicine. Water purification technologies like electrodialysis rely on the electrolytic flow properties. This short and by far not exhaustive list of occurrences of electrolytic flow processes shows the importance of correct modeling of electrolyte flows. Due to the complex physical interactions present in this type of flows, in many cases numerical simulation techniques are required to facilitate a deeper understanding of the flow behavior.

This contribution introduces a coupled modeling and simulation approach which has several new aspects. Section 2 reviews a modeling approach which uses recently obtained formulations [DGM13] based on first principles of nonequilibrium thermodynamics. It allows to include ion-solvent interactions, finite ion size and solvation effects in a consistent manner. At the end of this section, a short overview over existing analytical results is given. Section 3 starts with an overview on previous results on numerical methods. It introduces a finite volume discretization approach for ion transport in a self-consistent electric field which is motivated by results from semiconductor device simulation and has been adapted to the improved ion transport models [Fuh16]. For fluid flow, the recently developed [Lin14] pressure robust mixed finite element method is introduced. The section is finalized by a short description of the fix point approach for coupling flow and charge transport. Section 4 provides the results of a number of numerical examples which verify the presented approach and exhibit its potential for further research.

## 2 Continuum models

Electroosmotic flows are characterized by the presence of an electric field that exerts a net force on the fluid molecules in regions where the local net charge due to the ions present therein is nonzero. Being part of the momentum balance for the barycentric velocity of the fluid, this net force induces fluid motion. Correspondingly, the dissolved ionic species molecules in the fluid are advected by the barycentric velocity field. Motion of ions relative to the barycentric velocity is induced by the gradients of their chemical potential and the electrostatic potential. A counterforce to the motion of dissolved molecules is due to elastic interactions between the ions and the solvent.

In addition to these processes, the spatial distribution of the net charge of ions in a self-consistent way contributes to the electric field.

Classical models for electrolytes [Ner88, Pla90] rely on a *dilute solution* assumption. In this case the ion-solvent interaction is neglected. As a result, there is no mechanism to limit the accumulation of ions inside narrow boundary layers that screen the electric field at electrodes or charged walls, see Fig. 1.

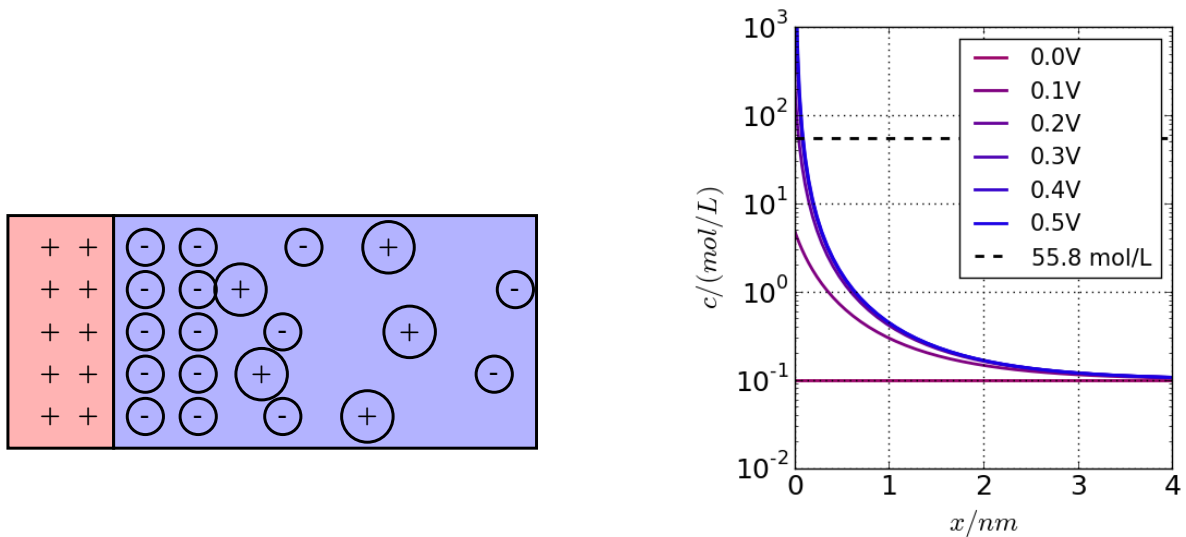


**Fig. 1** Left: accumulation of negative ions at positively charged electrode surface. Right: already for moderate applied voltages, the classical Nernst-Planck model, which ignores the ion-solvent interaction, predicts ion concentrations at an ideally polarizable electrode which are significantly larger than the molar density of the solvent – in this case water with a molar density of  $55.8 \text{ mol/dm}^3$ .

## 2.1 Bulk equations

The limitations of classical models are well known and several remedies for these shortcomings have been suggested early on [Ste24]. Here a model for the flow of electrolytes is considered which has been introduced in [DGM13, DGL14, LGD16] based on consistent application of the principles of nonequilibrium thermodynamics [dGM62]. It includes ion volume and solvation effects and consistently couples the transport equations to the momentum balance and generalizes previous approaches to include steric (ion size) effects [Bik42, Fre52, CS69, MCSJ71, KV81], see also [KBA07].

In a given bounded space-time domain  $\Omega \times (0, t^\#) \subset \mathbb{R}^d \times (0, \infty)$ , and with appropriate initial and boundary conditions, the system (1a)–(5c) describes the isothermal evolution of the molar concentration of  $N$  charged species  $c_1 \dots c_N$  with charge numbers  $z_1 \dots z_N$  dissolved in a solvent of concentration  $c_0$ . Species are further characterized by their molar volumes  $v_i$  and molar masses  $M_i$ .

The electric field is described as the gradient of the electrostatic potential  $\psi$ . The barycentric velocity of the mixture is denoted by  $\mathbf{u}$ , and  $p$  is the pressure. The following equations are considered:

$$\partial_t(\rho \mathbf{u}) - \nu \Delta \mathbf{u} + \rho(\mathbf{u} \cdot \nabla) \mathbf{u} + \nabla p = q \nabla \psi \quad (1a)$$

$$\nabla \cdot \rho \mathbf{u} = 0 \quad (1b)$$

$$\partial_t c_i + \nabla \cdot (\mathbf{N}_i + c_i \mathbf{u}) = 0 \quad (i = 1 \dots N) \quad (1c)$$

$$-\nabla \cdot (\varepsilon \nabla \psi) = F \sum_{i=1}^N z_i c_i = q. \quad (1d)$$

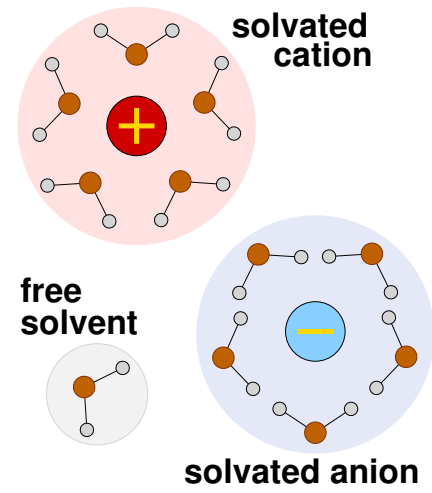
Equation (1a) together with (1b) comprises the incompressible Navier–Stokes equations for a fluid of viscosity  $\nu$  and constant density  $\rho$ . In the general case, where molar volumes and molar masses are not equal,  $\rho$  would depend on the local composition of the electrolyte.

In regions where the space charge  $q = F \sum_{i=1}^N z_i c_i$  ( $F$  being the Faraday constant) is nonzero, the electric field  $\nabla \psi$  becomes a driving force of the flow.

The partial mass balance equations (1c) describe the redistribution of species concentrations due to advection in the velocity field  $\mathbf{u}$  and molar diffusion fluxes  $\mathbf{N}_i$ . The Poisson equation (1d) describes the distribution of the electrostatic potential  $\psi$  under a given configuration of the space charge. The constant  $\varepsilon$  is the dielectric permittivity of the medium.

The fluxes  $\mathbf{N}_i$ , the molar chemical potentials  $\mu_i$  and the incompressibility constraint for a liquid electrolyte are given by

**Fig. 2** Constituents of the liquid electrolyte are the free solvent molecules and solvated ions, i.e. larger complexes that are build from a center ion and a solvation shell of bounded polar solvent molecules.



$$\mathbf{N}_i = -\frac{D_i}{RT} c_i \left( \nabla \mu_i - \frac{\kappa_i M_0 + M_i}{M_0} \nabla \mu_0 + z_i F \nabla \psi \right) \quad (i = 1 \dots N) \quad (2a)$$

$$\mu_i = (\kappa_i v_0 + v_i)(p - p^\circ) + RT \ln \frac{c_i}{\bar{c}} \quad (i = 0 \dots N) \quad (2b)$$

$$1 = v_0 c_0 + \sum_{i=1}^N (\kappa_i v_0 + v_i) c_i. \quad (2c)$$

The generalized Nernst-Planck flux (2a) combines the gradients of the species chemical potentials  $\nabla \mu_i$ , the gradient of the solvent chemical potential  $\nabla \mu_0$  and the electric field  $\nabla \psi$  as driving forces for the motion of ions of species  $i$  relative to the barycentric velocity  $\mathbf{u}$ . In this equation,  $D_i$  are the diffusion coefficients,  $R$  is the molar gas constant, and  $T$  is the temperature. Equation (2b) is a constitutive relation for the chemical potential  $\mu_i$  depending on the local pressure and concentration. Here,  $p^\circ$  is a reference pressure, and  $\bar{c} = \sum_{i=0}^N c_i$  is the summary species concentration. In (2c) a simple model for solvated ions is applied, see [DGL14, Fuh16, DGLM17]. In polar solvents like water, ions carry a shell of electrically attracted solvent molecules, see Fig. 2. As a result, the mass and volume of a solvated ion are given by  $\kappa_i M_0 + M_i$  and  $\kappa_i v_0 + v_i$ , respectively. The incompressibility constraint (2c) limits the accumulation of ions in the polarization boundary layer to physically reasonable values, see Fig. 3. For typical boundary conditions, the reader is referred to numerical example section 4.

Comparing the constitutive equations (5a)-(5c) to the classical Nernst-Planck flux [Ner88, Pla90]

$$\mathbf{N}_i = -D_i \left( \nabla c_i + z_i c_i \frac{F}{RT} \nabla \psi \right) \quad (i = 1 \dots N), \quad (3)$$

which considers dilute solutions, one observes that in (3) the ion-solvent interaction described by the term  $\nabla \mu_0$  is ignored. Moreover in (3) implicitly a material model is assumed that neglects the pressure dependence of  $\mu_i$ , which is inappropriate in charged boundary layers, see Fig. 1, right.

The mass density of the mixture is

$$\rho = M_0 c_0 + \sum_{i=1}^N (\kappa_i M_0 + M_i) c_i = \frac{M_0}{v_0} + \sum_{i=1}^N \left( M_i - M_0 \frac{v_i}{v_0} \right) c_i. \quad (4)$$

As for reasonable solvation numbers  $\kappa_i \approx 10$ , the density  $\rho$  is dominated by the density of the solvent  $\rho_0 = \frac{M_0}{v_0}$ , for simplicity, and due to the fact that the pressure robust Navier-Stokes solver described in Section 3.3 currently is available only for constant density  $\rho$ , in the sequel it is assumed that all species molar masses and molar volumes are equal:  $v_i = v_0$ ,  $M_i = M_0$  ( $i = 1 \dots N$ ), leading to

$$\mathbf{N}_i = -\frac{D_i}{RT} c_i \left( \nabla \mu_i - (\kappa_i + 1) \nabla \mu_0 + z_i F \nabla \psi \right) \quad (i = 1 \dots N) \quad (5a)$$

$$\mu_i = v_0 (\kappa_i + 1) (p - p^\circ) + RT \ln \frac{c_i}{\bar{c}} \quad (i = 0 \dots N) \quad (5b)$$

$$1 = v_0 c_0 + \sum_{i=1}^N (\kappa_i + 1) v_0 c_i. \quad (5c)$$

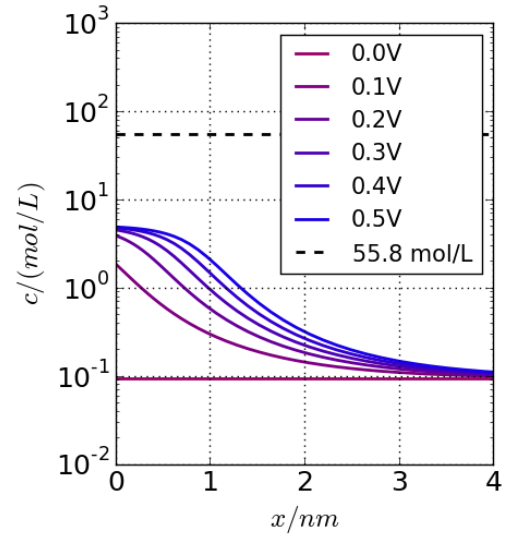


**Fig. 3** Physically reasonable ion concentrations at ideally polarizable electrode in equilibrium for the generalized Nernst-Planck flux (5a).

## 2.2 Reformulation in species activities

In order to develop a space discretization approach for the generalized Nernst-Planck fluxes (5a), after [Fuh15], the system is re-formulated in terms of (effective) species activities  $a_i = \exp\left(\frac{\mu_i - (\kappa_i + 1)\mu_0}{RT}\right)$ . The quantity  $\mu_i - (\kappa_i + 1)\mu_0$  is sometimes denoted as entropy variable [Jün15]. Introducing the activity coefficients  $\gamma_i = \frac{a_i}{c_i}$  and its inverse (reciprocal)  $\beta_i = \frac{1}{\gamma_i} = \frac{c_i}{a_i}$  allows to transform the Nernst-Planck-Poisson system consisting of (1c), (1d), (5a) to

$$-\nabla \cdot (\varepsilon \nabla \psi) = F \sum_{i=1}^N z_i \beta_i a_i = q. \quad (6a)$$

$$0 = \partial_t(\beta_i a_i) + \nabla \cdot (\mathbf{N}_i + \beta_i a_i \mathbf{u}) \quad (i = 1 \dots N) \quad (6b)$$

$$\mathbf{N}_i = -D_i \beta_i \left( \nabla a_i + a_i z_i \frac{F}{RT} \nabla \psi \right) \quad i = (1 \dots N). \quad (6c)$$

From (5b) and (5c) one obtains

$$a_i = \frac{v_0 \beta_i a_i}{1 - v_0 \sum_{j=1}^N \beta_j a_j (\kappa_j + 1)} \quad (i = 1 \dots N)$$

which is a linear system of equations which allows to express  $\beta_1 \dots \beta_n$  through  $a_1 \dots a_n$ . It has the unique solution [Fuh15]

$$\beta_i = \beta = \frac{1}{v_0 + v_0 \sum_{j=1}^N a_j (\kappa_j + 1)} \quad (i = 1 \dots N). \quad (7)$$

It follows immediately that for any nonnegative solution  $a_1 \dots a_n$  of system (6), the resulting concentrations are bounded in a physically meaningful way:

$$0 \leq c_i = \beta_i a_i \leq \frac{1}{v_0}. \quad (8)$$

A similar observation in the context of cross diffusion systems has been described in [Jün15].

In the general case with different molar volumes and molar masses, system (7) becomes nonlinear, the quantities  $\beta_i$  differ between species and in addition depend on the pressure  $p$  [Fuh15, Fuh16], leading to a nonlinear system of equations

$$\beta_i = B_i(a_1 \dots a_n, \beta_1 \dots \beta_n, p) \quad (i = 1 \dots N). \quad (9)$$

## 2.3 Analytical treatment

Long before the advent of computers, the need to understand mechanisms of electrokinetic phenomena like electroosmosis and electrophoresis led to the development of various asymptotic and analytical tools to handle these complex effects, mostly relying on the classical Nernst-Planck fluxes. Fundamental in this context is the Helmholtz-Smoluchowski theory [Smo21] which quantitatively explains the electroosmotic flow phenomenon. For comprehensive treatment see e.g. [Duk74, Lyk05, Hun13]. See also section 4.1 of this contribution for a short overview.

A particular intriguing phenomenon from the mathematical and application point of view is the development of electroconvective instabilities in electrodialysis cells [RZ00, DZR<sup>+</sup>11].

Apparently, mathematical existence and uniqueness theory started much later. In the case of the classical Nernst-Planck flux, existence of a local solution has been established in [Jer02]. Existence, and in some cases uniqueness of solutions has been proven in [Ryh06, Ryh09, Sch09]. In [BFS14], the existence of unique local strong solutions in bounded  $n$ -dimensional domains as well as the existence of unique global strong solutions and exponential convergence to uniquely determined steady states in two space dimensions has been proven. The authors of [C18] prove global existence and stability results for large data in two space dimension. In [FS17], global weak solutions in three space dimensions are constructed. Recently, existence theory for the improved model in the case of a compressible flow has been developed in [DDGG17a, DDGG17b, DDGG17c].

An analytical solution of the Poisson–Nernst–Planck–Stokes equations in a cylindrical channel has been derived in [BF11] in the context of fuel cell membranes.

## 3 Numerical methods

### 3.1 Previous work

A number of contributions is devoted to the discretization and numerical solution for the case of the classical Nernst-Planck flux. The authors of [PS10] consider a finite element discretization of the coupled system. A mixed finite element method for the 2D Stokes-Nernst-Planck-Poisson system is considered in [FRK11]. A similar approach is used in [KFND10]. In [DSP11, CDS12], a Galerkin pseudospectral method is used to perform simulations of electrokinetic instabilities over permselective membranes in a rectangular domain. For a similar problem, the authors of [PLL<sup>+</sup>12] apply a finite volume method for both the Navier-Stokes and the Nernst-Planck-Poisson subsystems, coupling them via a fixed point iteration method. The authors of [DAM13] apply a finite difference method. In [NKU<sup>+</sup>14], a rather recent overview on the state of the art for this problem class is given. In [HS18], a mixed finite element method is considered and analyzed. Finite difference methods are used e.g. in [LFY02], [DOS05] and in [WPC<sup>+</sup>09] for a micro/nanofluidic applications. Extension to the nonisothermal case is considered in [TYCG03] using a finite volume scheme on a regular grid in cylindrical coordinates. A three-dimensional model including thermal and mechanical effects based on an edge averaged exponentially fitted finite element method with applications in membrane biology is described in [SAMJ17].

An interesting comparison between a custom developed and a commercially available simulation tool one finds in [KDM15]. The commercially available code COMSOL Multiphysics is used to obtain numerical results on electroosmotic flows in [AZJ<sup>+</sup>10] and [PSD<sup>+</sup>11]. The authors of [RDHdG16] modified the Coulomb force term in (1a) by adding the sum of the concentration gradients in order to minimize spurious flows due to large pressure gradients and implemented this approach into COMSOL Multiphysics, see also section 4.4 of this contribution.

Coupling between fluid flow and modified Poisson-Nernst-Planck models taking into account steric effects up to now has been considered only by very few authors. In [BB14], a constant flow situation for a modified Nernst-Planck flux along a pore is assumed, allowing to decouple the problem. In order to model the behavior of ionic liquids, a simple upwind finite volume method on a rectangular grid to discretize the modified Poisson-Nernst-Planck equations according to [KBA07] has been coupled to the lattice Boltzmann method for the Navier-Stokes equations in [WBPS17]. The authors of [RM17] implemented a 2D numerical model of a nanopore with reservoirs into ANSYS Fluent.

In the sequel, a coupling approach is presented which combines novel, pressure robust mixed finite element methods [Lin14, JLM<sup>+</sup>17] with a thermodynamically consistent two point flux finite volume method designed for the discretization of modified Nernst-Planck-Poisson equations using ideas from semiconductor device simulation.

### 3.2 Thermodynamically consistent finite volume methods for species transport

A two point flux finite volume method on boundary conforming Delaunay meshes is used to approximate the Nernst-Planck-Poisson part of the problem. It has been inspired by the successful Scharfetter-Gummel box method for the solution of charge transport problems in semiconductors [SG69, BRF83]. For a recent overview on this method see [FRD<sup>+</sup>17]. It was initially developed for drift-diffusion problems in non-degenerate semiconductors exhibiting Boltzmann statistics for charge carrier densities whose fluxes are equivalent to the classical Nernst-Planck flux (3).

The simulation domain  $\Omega$  is partitioned into a finite number of closed convex polyhedral control volumes  $K \in \mathcal{K}$  such that  $K \cap L = \partial K \cap \partial L$  and  $\bar{\Omega} = \bigcup_{K \in \mathcal{K}} K$ . With each control volume a node  $\mathbf{x}_K \in K$  is associated. If the control volume intersects with the boundary  $\partial\Omega$ , its corresponding node shall be situated on the boundary:  $\mathbf{x}_K \in \partial\Omega \cap K$ . The partition shall be *admissible* [EGH00], that is for two neighboring control volumes  $K, L$ , the edge  $\overline{\mathbf{x}_K \mathbf{x}_L}$  is orthogonal to the interface between the control volumes  $\partial K \cap \partial L$ . Let  $\mathbf{h}_{KL} = \mathbf{x}_L - \mathbf{x}_K$  and  $h_{KL} = |\mathbf{h}_{KL}|$ . Then, the normal vectors to  $\partial K$  can be calculated as  $\mathbf{n}_{KL} = \frac{1}{h_{KL}} \mathbf{h}_{KL}$ .

A constructive way to obtain such a partition is based on the creation of a boundary conforming Delaunay triangulation resp. tetrahedralization of the domain and the subsequent construction of its dual, the Voronoi tessellation intersected with the domain, see e.g. [BRF83, SGF10, FRD<sup>+</sup>17], see also Fig. 4.

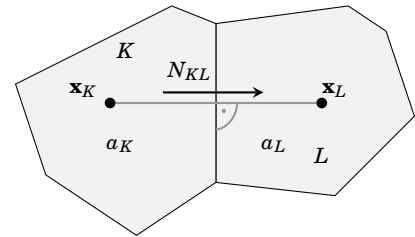


**Fig. 4** Two neighboring control volumes  $K$  and  $L$  with collocation points  $\mathbf{x}_K, \mathbf{x}_L$  stored activities  $a_K, a_L$  and flux  $N_{KL}$ .

The time axis is subdivided into intervals

$$0 = t^0 < t^1 < \dots < t^{N_t} = t^\sharp.$$

Denote by  $\mathbf{J}_i = c_i \mathbf{u} + \mathbf{N}_i = \beta_i a_i \mathbf{u} + \mathbf{N}_i$  the convection diffusion flux of the model under consideration. The general approach to derive a two point flux finite volume scheme for a conservation law

$$\partial_t c_i + \nabla \cdot \mathbf{J}_i = 0$$

consists in integrating the equation over a space-time control volume  $K \times [t^{n-1}, t^n]$  (index  $i$  omitted):

$$\begin{aligned} 0 &= \int_{t^{n-1}}^{t^n} \int_K (\partial_t c + \nabla \cdot \mathbf{J}) d\mathbf{x} dt = \int_{t^{n-1}}^{t^n} \int_K \partial_t c d\mathbf{x} dt + \int_{t^{n-1}}^{t^n} \int_{\partial K} \mathbf{J} \cdot \mathbf{n} ds dt \\ &= \int_K (c^n - c^{n-1}) d\mathbf{x} + \sum_{L \text{ neighbor of } K} \int_{t^{n-1}}^{t^n} \int_{\partial K \cap \partial L} \mathbf{J} \cdot \mathbf{n}_{KL} ds dt \end{aligned}$$

This is approximated via

$$|K| \frac{c_K^n - c_K^{n-1}}{t^n - t^{n-1}} + \sum_{L \text{ neighbor of } K} |\partial K \cap \partial L| J_{KL}^n = 0,$$

and it remains to define the numerical fluxes  $J_{KL}^n$  which should approximate the continuous fluxes between two neighboring control volumes and depend on the unknown values in the two collocation points  $\mathbf{x}_K$  and  $\mathbf{x}_L$  at moment  $t^n$  in order to obtain a fully implicit in time scheme.

The modification of the Scharfetter-Gummel scheme [SG69] proposed in [Fuh15] is based on the similarity of the expressions (6c) and (3) up to the pre-factor  $\beta$ . The later is the same as the drift-diffusion flux in non-degenerate semiconductors,

for which this discretization scheme was initially derived. Let  $B(\xi) = \frac{\xi}{e^\xi - 1}$  be the Bernoulli function. Set

$$J_{KL} = D\beta_{KL} \cdot \frac{B(-\delta_{KL} - \frac{u_{KL}}{D})\alpha_K - B(\delta_{KL} + \frac{u_{KL}}{D})\alpha_L}{h_{KL}}$$

where  $\beta_{KL}$  is an average of the inverse activity coefficients  $\beta_K$  and  $\beta_L$ ,  $\delta_{KL} = \frac{zF}{RT}(\psi_K - \psi_L)$  is proportional to the local electric force, and

$$u_{KL} = \int_{\partial K \cap \partial L} \mathbf{u} \cdot \mathbf{h}_{KL} ds \quad (10)$$

is the normal integral over the interface  $\partial K \cap \partial L$  of the convective flux scaled by  $h_{KL}$ . If the continuous flux is divergence free, i.e. it fulfills equation (1b), the flux projections  $u_{KL}$  fulfill the discrete divergence condition

$$\sum_{L \text{ neighbor of } K} |\partial K \cap \partial L| u_{KL} = 0 \quad (11)$$

which in the absence of charges and coupling through the activity coefficients guarantees a discrete maximum principle of the approximate solution [FLL11].

The resulting time discrete implicit Euler finite volume upwind scheme guarantees nonnegativity of discrete activities and exact zero fluxes under thermodynamic equilibrium conditions. Moreover it guarantees the bounds (8) [Fuh15].

Existence and convergence theory for the discrete problem for generalized Nernst-Planck fluxes is still open. For cases similar to the classical Nernst-Planck fluxes, in one space dimension, an independent derivation, and second order convergence in the discrete maximum norm for the Scharfetter-Gummel scheme has been shown in [Il'69]. Under the assumption that second derivatives of the continuous solution exist, in [LMV96] for moderately sized drift terms and two-dimensional, square grids, second order convergence for the scheme in the  $L_2$ -norm has been shown. Re-interpretations of the finite volume Scharfetter-Gummel scheme as a nonstandard finite element method allowed to obtain convergence estimates schemes on Delaunay grids [MW94, XZ99]. For a general approach to the convergence theory of finite volume schemes, see [EGH00]. In [EFG06], weak convergence (no order estimate) for a generalization of the Scharfetter-Gummel scheme to nonlinear convection-diffusion problems has been shown, however, this proof does not cover the case of the generalized Nernst-Planck flux.

The discretization ansatz leads to a large nonlinear discrete system in the unknowns  $\psi, a_1 \dots a_n$  which is solved by Newton's method in every time step. For the general model, the nonlinear equations for the inverse activity coefficients  $\beta_1 \dots \beta_n$  according to (9) and a Laplace equation for the pressure have to be added to the overall system [Fuh16].

### 3.3 Pressure robust, divergence free finite elements for fluid flow.

For a recent and comprehensive introduction into the field of finite element methods for incompressible flow, see e.g. [Joh16]. Mixed finite element methods approximate the Stokes resp. Navier–Stokes equations based on an inf-sup stable pair of velocity ansatz space  $V_h$  and pressure ansatz space  $Q_h$ . A fundamental property of the Stokes and Navier–Stokes equations consists in the fact that — under appropriate boundary conditions — the addition of a gradient force to the body force on the right-hand side of the momentum balance (1a) leaves the velocity unchanged, as it just can be compensated by a change in the pressure. Most classical mixed finite element methods for the Navier–Stokes equations do not preserve this property [GR12]. As a consequence, the corresponding error estimates for the velocity depend on the pressure [Joh16]. Moreover, the divergence constraint of the discrete solution  $\mathbf{u}_h$  is fulfilled only in a weak finite element sense:

$$\int_{\Omega} q_h \operatorname{div}(\mathbf{u}_h) dx = 0 \quad \text{for all } q_h \in Q_h. \quad (12)$$

This raises problems when coupling the flow simulation to a transport simulation using finite volume methods, because the maximum principle for the species concentration is directly linked to the divergence constraint in the finite volume sense (11) [FLL11].

Pressure robust mixed methods, first introduced in [Lin14], are based on the introduction of a divergence free velocity reconstruction  $\Pi$  into the discrete weak formulation of the flow problem. The resulting discretization of the stationary Stokes equation (provided here for simplicity) reads as: find  $(\mathbf{u}_h, p_h) \in V_h \times Q_h$  such that

$$\int_{\Omega} v \nabla \mathbf{u}_h : \nabla \mathbf{v}_h dx + \int_{\Omega} p \nabla \cdot \mathbf{v}_h dx = \int_{\Omega} \mathbf{f} \cdot (\Pi \mathbf{v}_h) dx \quad \text{for all } \mathbf{v}_h \in V_h$$

$$\int_{\Omega} q_h \nabla \cdot \mathbf{u}_h dx = 0 \quad \text{for all } q_h \in Q_h.$$

This formulation differs from that of the classical mixed methods only in the introduction of a *reconstruction operator*  $\Pi$  with the following properties:

- (i) If  $\mathbf{u}_h$  is divergence free in the weak finite element sense (12), then the reconstruction  $\Pi \mathbf{u}_h$  is pointwise divergence free in the continuous sense:

$$\nabla \cdot (\Pi \mathbf{u}_h) = 0.$$

- (ii) The change of the test function by the reconstruction operator causes a consistency error that should have the same asymptotic convergence rate of the original method and should not depend on the pressure.

Under these conditions, the resulting velocity error estimate is independent of the pressure [JLM<sup>+</sup>17]. Furthermore, using the reconstruction  $\Pi \mathbf{u}_h$  in the coupling to the discretization of the ion flux guarantees the divergence condition (11) for the projections obtained via (10). Using this method, even for a complicated structure of the pressure as in the case of electrolyte flows, a good velocity approximation can be obtained without the need to resort to high order pressure approximations. This leads to a significant reduction of degrees of freedom numbers necessary to obtain a given accuracy of the velocity. The action of  $\Pi$  on a discrete velocity field can be calculated locally, on elements or element patches. Therefore its implementation leads to low overhead in calculations.

For a comprehensive overview on this method, and the role of the divergence constraint in flow discretizations, see the survey article [JLM<sup>+</sup>17].

### 3.4 Coupling strategy.

The coupling approach between the Navier–Stokes solver and the Nernst-Planck-Poisson solver is currently based on a fixed point iteration strategy:

```

Set  $\mathbf{u}_h, p_h$  to zero, calculate initial solution for (1d)–(5c);
while not converged do
    Provide  $\psi_h, q_h$  to Navier–Stokes solver;
    Solve (1a)–(1b) for  $\mathbf{u}_h, p_h$ ;
    Project  $\Pi \mathbf{u}_h, p_h$  to the Poisson-Nernst-Planck solver;
    Solve (6a)–(6c);
end

```

The projection of  $\Pi \mathbf{u}$  to the finite volume solver according to (10) includes the integration of the reconstructed finite element solution  $\Pi \mathbf{u}_h$  over interfaces between neighboring control volumes of the finite volume method. For a detailed explanation of this algorithmically challenging step see [FLL11]. Sufficient accuracy of this step guarantees that the projected velocity is divergence free in the sense (11). In the implementation, the integrals are calculated by quadrature rules, and for a given discretization grid, the projection operator is assembled into a sparse matrix, allowing for computationally efficient repeated application of the projection operator during the fixed point iteration. As a consequence, in the case of electroneutral, inert transported species, the maximum principle for species concentrations is guaranteed [FLL11]. In combination with pressure robust finite element methods, this coupling approach was first applied to modeling of thin layer flow cells [MFL<sup>+</sup>16].

## 4 Numerical examples

In this section, first stationary simulation results based on the coupled method are presented which are mainly intended to verify the correctness of the method and its implementation.

The discretization methods and the coupling strategy introduced above are implemented in the framework of the toolbox `pdelib` [JF<sup>+</sup>18] that is developed at WIAS. In the following examples the solution of the Nernst-Planck-Poisson system is performed using Newton's method with full analytical Jacobians combined with parameter embedding to tackle strong nonlinearities starting with the equilibrium solution, for details, see e.g. [FRD<sup>+</sup>17]. For the flow part of the problem, the stationary Stokes solution was solved using a second order finite element method. Its velocity space consists of piecewise quadratic continuous vector fields enhanced with cell bubble functions and its pressure space consists of piecewise linear and discontinuous scalar fields [BR85]. This method allows for an easy divergence free reconstruction operator into the Raviart-Thomas finite element space of first order by standard interpolation [LM16, JLM<sup>+</sup>17]. Linear systems were solved using the sparse direct solver Pardiso [SG04, SG<sup>+</sup>17].

#### 4.1 Infinite pore with charged walls

For an extensive treatment of this case for the classical Nernst-Planck-Poisson flux, see [Hun13]. As similar treatment one can find in [BB14]. Consider a stationary, laminar electroosmotic Stokes flow in an infinite domain under a constant in space applied electric field. Suppose that velocity and concentrations do not depend on the longitudinal coordinate  $z$ . This problem can be seen as a model of a pore of infinite length.

Let  $\Omega_\varnothing \subset \mathbb{R}^{d-1}$  be a convex cross-sectional domain and  $\Omega = \Omega_\varnothing \times \mathbb{R} \subset \mathbb{R}^d$ . Assume a constant flow along the  $z$ -Axis such that  $u_\varnothing = 0$ , and  $\partial_z u_z = 0$ . Set  $\psi = \psi_\varnothing + (z - z_0)E_z$  where  $E_z$  is the constant  $z$ -component of the electric field. Similarly, assume  $p = p_\varnothing + (z - z_0)\Pi_z$  where  $\Pi_z$  is the constant  $z$  component of the pressure gradient. These functions are linear in  $z$  and  $\nabla \cdot (\varepsilon \nabla \psi) = \nabla_\varnothing \cdot (\varepsilon \nabla_\varnothing \psi)$ . Further, consider zero ionic current in the cross sectional direction:  $N_{i,\varnothing} = 0$ .

From the momentum equation (1a) one obtains in  $\Omega_\varnothing$ :

$$\nabla_\varnothing p = q \nabla_\varnothing \psi \quad (13)$$

$$-\eta \Delta_\varnothing u_z + \Pi_z = q E_z. \quad (14)$$

Due to the assumptions on  $\mathbf{u}$ , (1b) is fulfilled, and, moreover,  $\nabla \cdot (\beta_i a_i \mathbf{u}) = 0$ . Then, together with the zero lateral current condition, and the fact that  $\mathbf{N}_z$  must be  $z$ -independent, the continuity equation (1c) is fulfilled. As its right hand side is independent on  $z$ , the Poisson equation (1d) gives

$$-\nabla_\varnothing \varepsilon \nabla_\varnothing \psi = q \quad (15a)$$

Finally, the zero lateral current condition reduces the Nernst-Planck equation (5a) to the equilibrium condition

$$a_i = \exp\left(\frac{z_i F}{RT}(\phi_i - \psi)\right) \quad (15b)$$

where  $\phi_i$  are constant electrochemical (quasi-Fermi) potentials which can be obtained from a bulk concentration condition [Fuh15]. As in [Fuh15], turn (13) into the second order equation

$$\Delta_\varnothing p(x, y) = \nabla_\varnothing \cdot (q \nabla_\varnothing \psi). \quad (15c)$$

With appropriate boundary conditions on  $\partial\Omega_\varnothing$

$$\varepsilon \partial_n \psi = \sigma \quad \partial_n p = q \partial_n \psi \quad (16a)$$

system (15a)-(15c) together with (7) corresponds to the equilibrium case described in [Fuh15] and can be generalized to the full model from [Fuh16].

Given the lateral charge distribution from the solution of (15a), equation (14) together with the no-slip boundary condition

$$u_z|_{\partial\Omega_\varnothing} = 0 \quad (17)$$

allows to calculate the lateral distribution of the velocity component  $u_z$  via the solution of an elliptic equation.

## 4.2 Slit between two infinite plates

For the case of flow in the slit of width  $2w$  between two infinite plates, set  $d = 2$ ,  $\Omega_\varnothing = (0, w)$ , and set symmetry boundary conditions at  $x = 0$  and a fixed pressure value:

$$\varepsilon \partial_x \psi(0) = 0, \quad p(0) = 0, \quad \eta \partial_x u_z(0) = 0 \quad (18)$$

From (15a) and (14) follows

$$\eta \partial_{xx} u_z = \varepsilon E_z \partial_{xx} \psi - \Pi_z. \quad (19)$$

Integrating once gives

$$\eta \partial_x u_z = \varepsilon E_z \partial_x \psi - \Pi_z x + C. \quad (20)$$

with  $C = 0$  due the boundary condition at  $x = 0$ . Let  $x_\zeta$  be such that  $u_z(x_\zeta) = 0$ . A second integration gives

$$\begin{aligned} \int_0^{x_\zeta} \eta \partial_x u_z dx &= \int_0^{x_\zeta} \varepsilon E_z \partial_x \psi - \Pi_z x dx \\ -\eta u_z(0) &= \varepsilon E_z (\psi(x_\zeta) - \psi(0)) - \Pi_z x_\zeta^2 \end{aligned}$$

Assuming  $\Pi_z = 0$ , i.e. that the pressure gradient is absent as the driving force, one can define the electroosmotic velocity  $v_{eo} = u_z(0)$ . Assuming that the pore width is sufficiently large to see a deviation from electroneutrality only in a small boundary layer close to  $x_\zeta$ , this is the velocity of the plug flow initiated by electroosmotic forces in the boundary layer. One obtains the famous Helmholtz-Smoluchowski formula [Smo21]

$$v_{eo} = -\frac{\varepsilon E_z \zeta}{\eta} \quad (21)$$

where  $\zeta = \psi(x_\zeta) - \psi(0)$  is the *zeta potential*. With the definition of the electrochemical potentials  $\phi_i$  from molarity and electroneutrality one can assume  $\psi(0) = 0$ . Moreover, for the flow model discussed in this example, with constant viscosity and no-slip boundary condition at the pore wall,  $x_\zeta = w$ , and  $\zeta = \psi|_{x=w}$  is the potential at the pore wall which is induced by the surface charge  $\sigma$ . Note that this derivation of the zeta potential does not depend on the particular variant of the Nernst-Planck flux.

Assuming the case of flow of a binary electrolyte in the slit between two infinite parallel plates, for the classical Nernst-Planck flux the zeta potential can be calculated explicitly and expressed by the Grahame equation [Hun13].

$$\zeta = \frac{2RT}{F} \operatorname{asinh} \left( \frac{\sigma}{\sqrt{8\varepsilon RT c_0}} \right), \quad (22)$$

where  $c_0 = c(0)$  is the bulk electrolyte concentration. In [Ove52, BN64], asymptotic theory is used to approximate the lateral distribution of the electrostatic potential and the flow velocity:

$$\psi(x) = \zeta \frac{\cosh \frac{x}{\lambda}}{\cosh \frac{w}{\lambda}}, \quad v_z(x) = v_{eo} \left( 1 - \frac{\cosh \frac{x}{\lambda}}{\cosh \frac{w}{\lambda}} \right), \quad (23)$$

where  $\lambda = \sqrt{\frac{\varepsilon RT}{2F^2 c_0}}$  is the Debye length. These expressions can be used to benchmark the implementation of numerical methods.

Using the finite volume method referenced in [Fuh15, Fuh16] to solve the modified Poisson-Boltzmann part, and a similar method to solve the equation for  $u_z$ , the slit problem is solved on a boundary layer grid such that  $h_{min} = 0.1 \text{ nm}/2.0^r$  close to  $x = w$   $h_{max} = 0.2w/2.0^r$  close to  $x = 0$  where  $r = 0, 1, \dots$  denotes the refinement level and such that subsequent intervals follow a geometric progression. Figure 5 shows the development of the plug flow profile for an increasing pore width  $w$ , and at the same time an increasing coincidence of the numerical solution with the asymptotic expression. Fig. 6 supports the verification of the accuracy of the numerical calculation of the zeta potential for the Gouy-Chapman model. One observes second order convergence to the value given by the Grahame equation (22) with respect to the number of grid points.

**Fig. 5** Comparison of simulation results with the classical asymptotic Helmholtz-Smoluchowski theory for different pore widths  $w$ . Depicted is the velocity component  $u_z$ . Lines: numerical solution of the cross-sectional problem. Dashed: approximation from [Ove52, BN64].

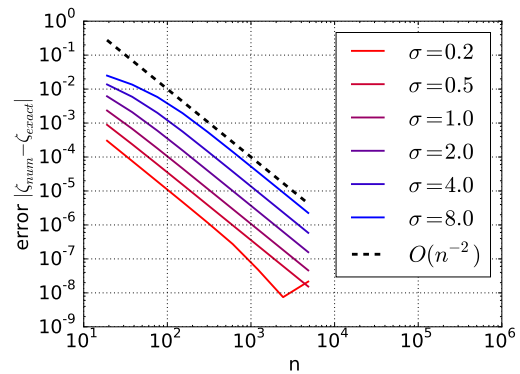
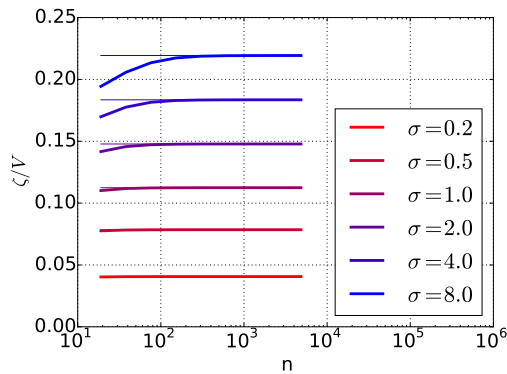
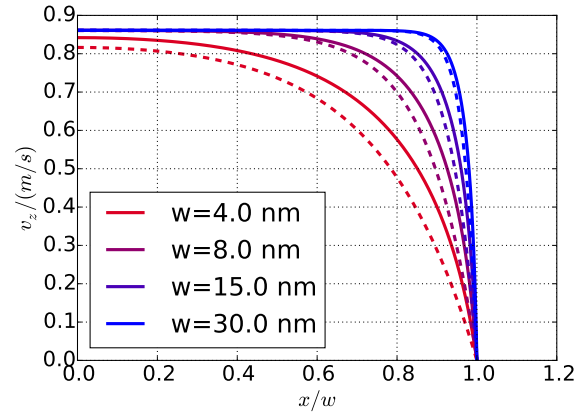


**Fig. 6** Result and accuracy of numerical zeta potential calculation for dilute solution model for a slit with half width 20nmvs. number of grid points. Left: Thin lines: value of zeta potential according to the Grahame equation (22), thick lines: numerically calculated zeta potential. Right: error vs. grid size.

### 4.3 Finite pore with charged walls

Now, consider a slit of width  $2w$  between two parallel plates of infinite width and finite length  $l$ . The geometry of this problem is represented by a rectangular domain  $(0, l) \times (0, w)$ . Let  $\Gamma_{in} = l \times (0, w)$ ,  $\Gamma_{out} = 0 \times (0, w)$ ,  $\Gamma_{wall} = (0, l) \times w$ ,  $\Gamma_{sym} = (0, l) \times 0$

In addition to the charged wall boundary conditions from Section 4.1, it is necessary to introduce boundary conditions at the inlet and the outlet.

Consider the coupled system consisting of (1a)–(1b) and (6a)–(6c) with two ionic species of opposite charges  $z_1 = 1$ ,  $z_2 = -1$ . Let  $v_0 = 1.0/M_w$ , where  $M_w = 55.8 \text{ mol/dm}^3$  is the molarity of liquid water at room temperature. Choose an activity value  $a_{res}$  such that  $c_{res} = \beta a_{res} = 1 \text{ mol/dm}^3$ . Then, set the following boundary conditions:

$$\begin{aligned}
 a_i|_{\Gamma_{in,out}} &= a_{res} & (i = 1, 2) & & \text{(Reservoir)} \\
 N_i \cdot \mathbf{n}|_{\Gamma_{wall}} &= 0 & (i = 1, 2) & & \text{(Impermeable wall)} \\
 \phi|_{\Gamma_{out}} &= 0V \\
 \phi|_{\Gamma_{in}} &= 0.5V & & & \text{(Applied electric field)} \\
 \varepsilon \nabla \phi \cdot \mathbf{n}|_{\Gamma_{wall}} &= \sigma = 10 \mu\text{A} \text{cm}^{-2} & & & \text{(Charged wall)} \\
 \mathbf{u}|_{\Gamma_{wall}} &= 0 & & & \text{(No-Slip)} \\
 \eta \nabla \mathbf{u} \cdot \mathbf{n}|_{\Gamma_{in,out}} &= p \mathbf{n} & & & \text{("Do nothing")}
 \end{aligned}$$

These inlet and outlet boundary conditions impose an electric field along the pore. They assume ion reservoirs of fixed concentration at both ends of the pore. Further, unhindered electrolyte flow into and out of the pore is assumed. At  $\Gamma_{sym}$ , set symmetry boundary conditions for all variables.

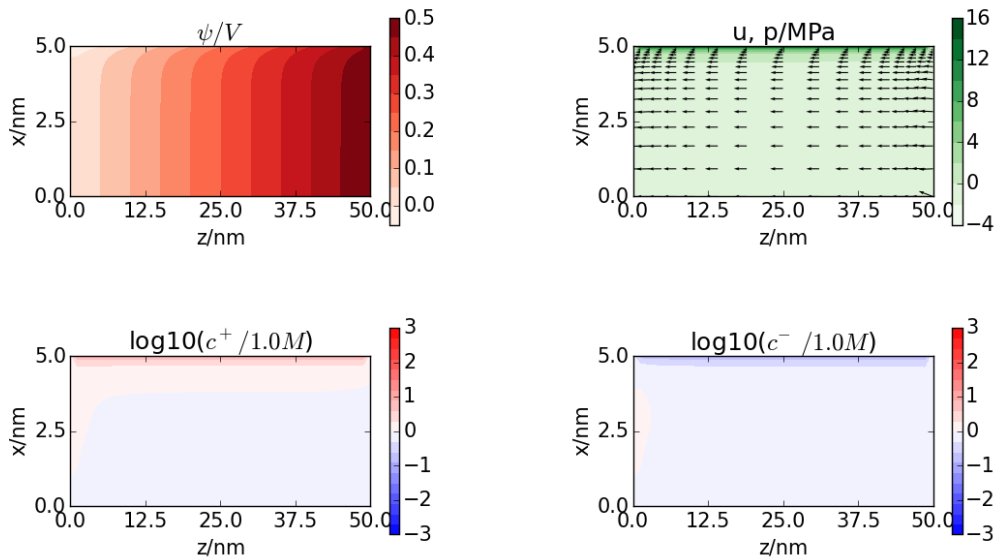


**Fig. 7** Electro-osmotic flow of an electrolyte with concentration  $1 \text{ mol/dm}^3$  through a straight nanopore of width  $10 \text{ nm}$  with charged walls for an imposed potential difference of  $0.5 \text{ V}$  in longitudinal direction. Top left: distribution of the electrostatic potential. Top right: velocity field (arrows) and pressure (color). Bottom row: positive resp. negative ion concentration.

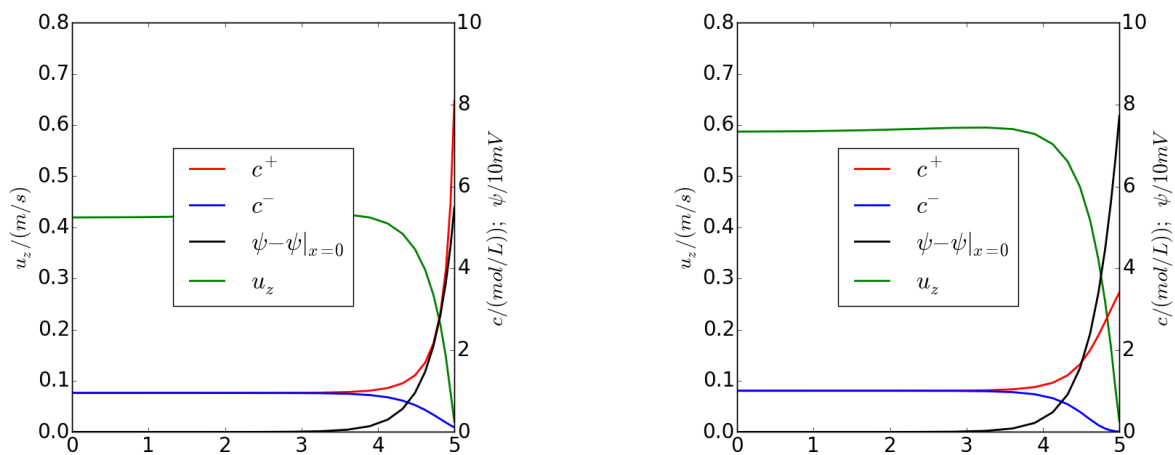


**Fig. 8** Velocity, concentration and electrostatic potential profiles in a  $10 \text{ nm}$  pore. Left: Classical Nernst-Planck model. Right: Improved model with solvation number  $\kappa = 10$ .

The solution for the classical Nernst-Planck model is depicted in Fig. 7 and 8 (left). It shows the onset of the typical plug flow behavior to be expected for electroosmotic flow in wider pores. Fig 8 at the same time demonstrates the influence of the model improvements discussed in this paper. Including the solvation effect increases the potential and decreases the concentrations at the charged wall boundary. As a consequence, the electroosmotic velocity increases.

In order to verify the coupling approach with the pressure robust Navier–Stokes solver, regard a second version of this problem, where for the velocity, periodic boundary conditions are considered. In order to avoid the edge effect for the species activities and the electrostatic potential at the reservoir boundaries, the solution of the 1D cross sectional Poisson-Boltzmann problem is taken as boundary value at the inlet resp. outlet. The problem is solved by the iterative procedure described in Algorithm 1. For this case of infinite slit boundary conditions Fig. 9 demonstrates a similar second order convergence rate of the zeta potential at point  $(w, \frac{l}{2})$  as for the one-dimensional case, cf. Fig. 6. Conversely, in the case of reservoir boundary conditions, the edge effect caused by the mismatch between the boundary conditions and the infinite slit situation leads to a lower convergence rate.

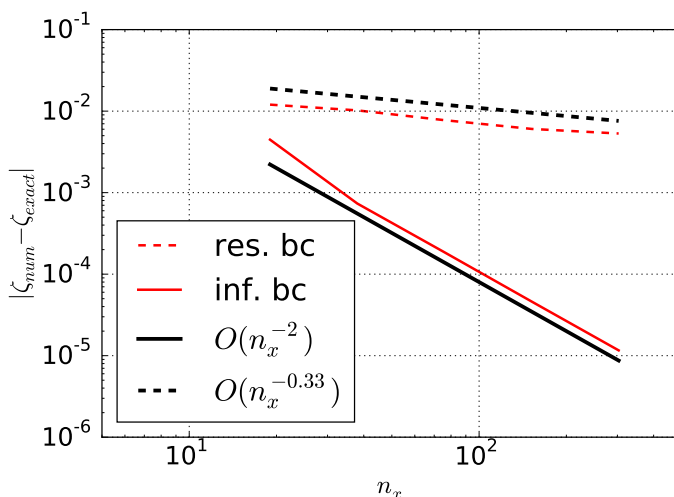


**Fig. 9** Error in zeta potential at the half length of the pore for Gouy-Chapman model for a pore of finite length vs. number of grid points in cross section direction. Lines: infinite slit boundary conditions. Dashed: reservoir boundary conditions.

#### 4.4 Spurious velocities in electrophoresis

The authors of [RDHdG16] discuss the occurrence of spurious velocities in mechanical equilibrium due to the pressure gradient failing to cancel the Coulomb force in the finite element approximation. As a consequence, a straightforward finite element discretization using standard mixed finite element methods results in spurious velocities in an equilibrium situation where both  $\mathbf{u} = \mathbf{0}$  and  $\mathbf{N}_i = \mathbf{0}$ , ( $i = 1 \dots n$ ). In order to remedy this situation, using the fundamental property of the Navier-Stokes equation mentioned at the beginning of section 3.3, they add the gradient force  $RT \sum_{i=1}^N \nabla c_i$  to the right hand side of the momentum balance (1a). In mechanical equilibrium, this indeed cancels out the pressure and removes the main source of spurious velocities.

While this approach appears to be a clever way to improve simulation results with existing software implementations (like COMSOL Multiphysics in [RDHdG16]), in the sequel it will be demonstrated that the coupled method presented in this paper without this modification delivers solutions with a similar or lower magnitude of spurious velocities.

In order to discuss this situation, regard a charged ( $1e/nm^2$ ) circle of radius  $10nm$  in a two-dimensional box of side length  $60nm$ . Assume symmetry boundary conditions at the side walls, charged wall and no-slip boundary conditions at the circle, reservoir, zero potential, reservoir and periodic flow boundary conditions at the top and bottom walls.

Fig. 10, bottom row shows directions and the absolute value of spurious velocities in equilibrium for three subsequent grid refinement levels, with logarithms of maximum values of the velocity  $-6.15$ ,  $-7.02$  and  $-8.07$ , respectively. In the top row, results are given for the case of flow simulation without the pressure robust correction. This corresponds to the results obtained in [RDHdG16] (see Fig. 5 therein), however an exact comparison is not possible due to lack of detail in the problem description in [RDHdG16].

For comparison, in Fig. 11 (right) the absolute value of the velocity and streamlines for an applied bias of  $0.1V$  are presented. For reference, in Fig. 11 (left), the level zero discretization grid is shown.

#### 4.5 Ionic current rectification and flow vortex in a conical nanopore

Consider the artificial conical nanopore described in [SF02, WBS10]. The length of the pore is  $12\mu m$ , the width of the small opening is  $3nm$ , the width of the large opening is  $300nm$ . Attached to the openings are reservoir regions which are both  $900nm$  wide and  $6\mu m$  long. The outer wall of the pore is charged with  $1As/m^2$ , and the bulk concentration of the electrolyte is  $0.1mol/dm^3$  resp.  $1mol/dm^3$ .

Experimental results documented in [SGS<sup>+</sup>02] (see e.g. Fig. 2 therein) show a significant rectification effect for the ionic current induced by potential differences of different signs applied between the reservoirs attached to the pore. Fig. 12 demonstrates this effect, the influence of coupling to the flow in the model, and the influence of the solvation on the simulation results. Fig. 12 (left) shows a significant rectification effect in the case of electrolyte concentration  $0.1mol/dm^3$ .

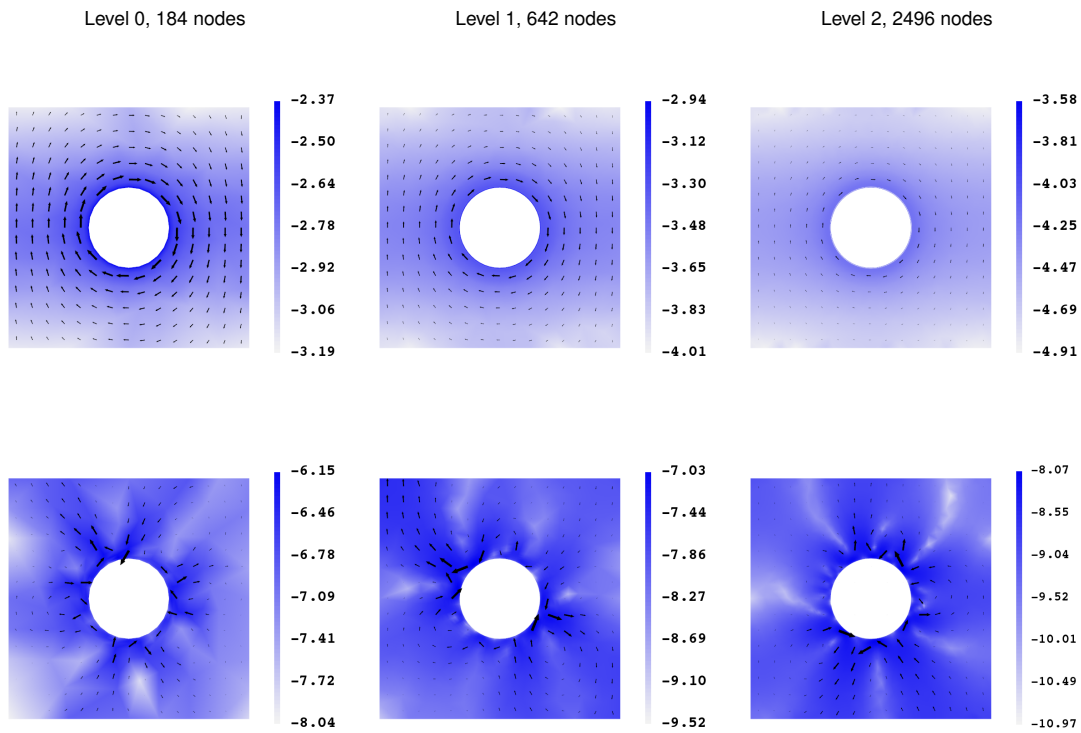


**Fig. 10** Absolute value (color, scale is  $\log_{10}(u/(m.s^{-1}))$ ) and arrow plots of velocities in equilibrium on coarse, middle and fine grids. Top row: classical mixed FEM. Bottom row: pressure robust FEM.

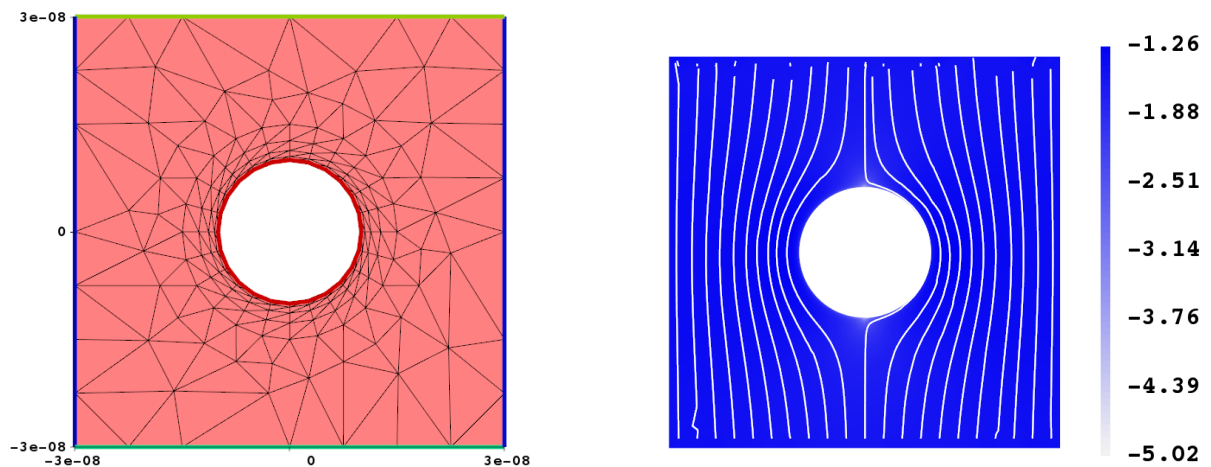


**Fig. 11** Left: coarsest, boundary adapted grid (184 nodes). Right: absolute value and streamlines of solution with applied bias of 0.1V on level 2 grid.

As expected, due to lower concentrations in the boundary layer, ionic currents for the full model with solvation are smaller than in the case of the classical Nernst-Planck flux. For electrolyte concentration  $1\text{mol}/\text{dm}^3$ , Fig. 12 (right) shows higher ionic currents, a diminished rectification effect.

Numerical simulations reported in [PSD<sup>+</sup>11] suggest the existence of a vortex stretched along the pore. For practical reasons, these have been performed on a “shortened” pore of length  $1\mu\text{m}$ . Fig. 13 demonstrates similar results for the pore geometry discussed here in the case of classical Nernst-Planck flux. One observes a vortex in the case of electrolyte concentration  $0.1\text{mol}/\text{dm}^3$ . According to Fig. 14, similar behavior is observed for the model with solvation, though in this case, the velocities are slightly larger than in the case without solvation. An explanation for this behavior may be the fact that according to (22), the zeta potential is inversely proportional to the square root of the concentration, therefore, for lower concentrations, there is a tendency to increase the electroosmotic flow velocity close to the wall. Fig 15 demonstrates this

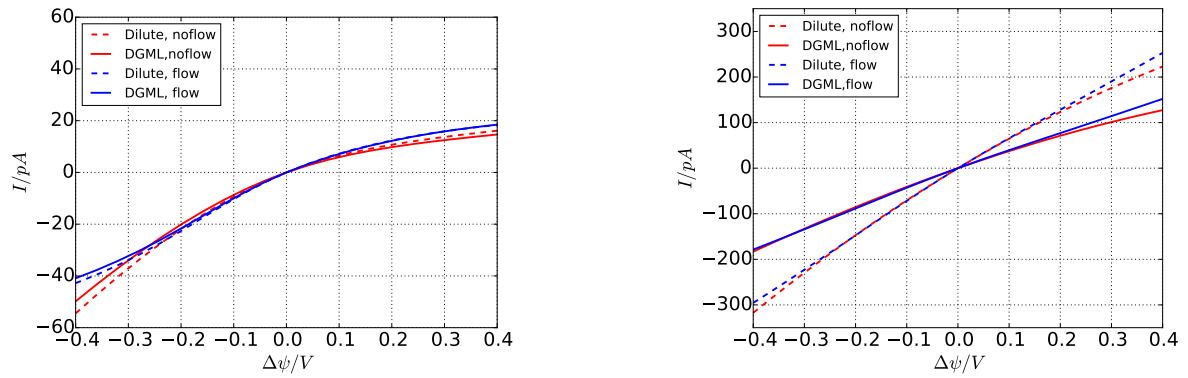


**Fig. 12** Simulated current rectification in a conical nanopore. Left: electrolyte concentration  $0.1\text{mol/dm}^3$ . Right: electrolyte concentration  $1\text{mol/dm}^3$ . DGML: model according to (2). Dilute: dilute solution model (3).

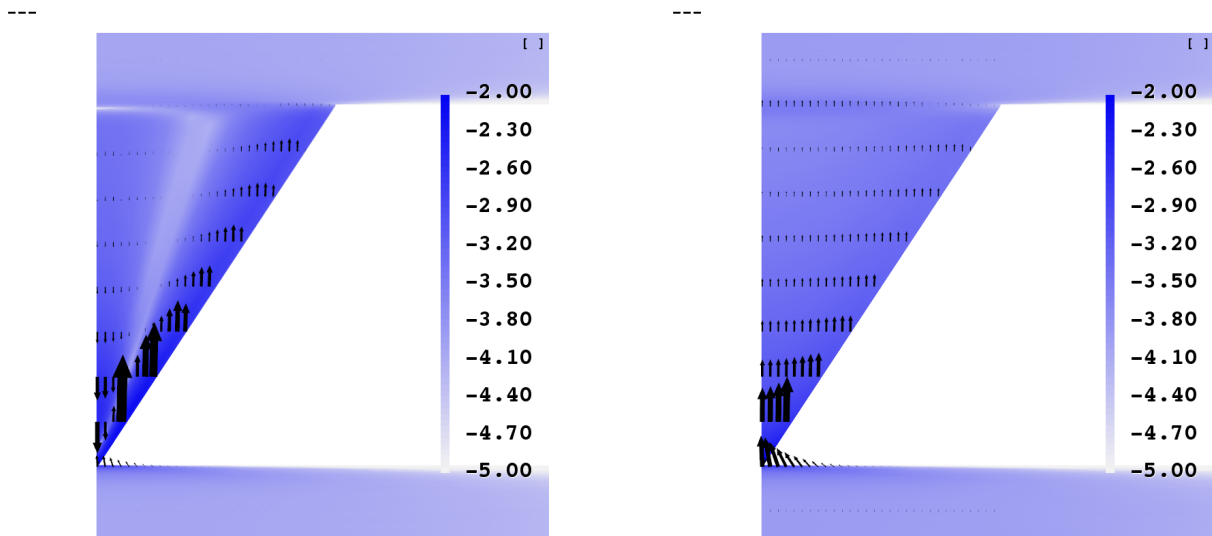


**Fig. 13** Simulated velocity field in a conical nanopore for classical Nernst-Planck flux. Color scale:  $\log||\mathbf{u}||$ . y axis compressed by factor of 27.

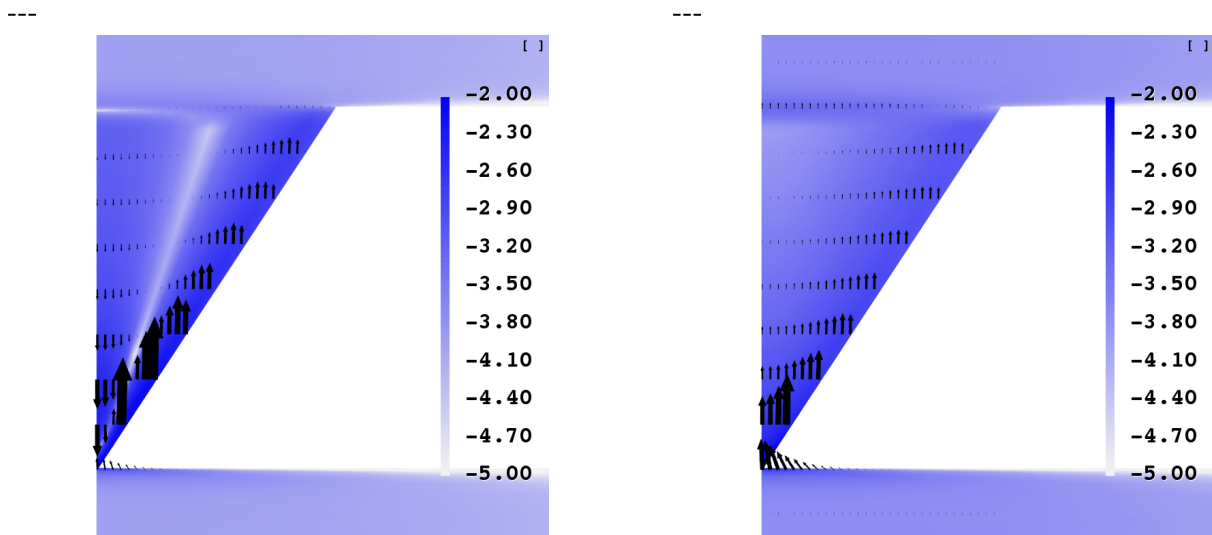


**Fig. 14** Simulated velocity field in a conical nanopore for Nernst-Planck flux with solvation effect. Color scale:  $\log||\mathbf{u}||$ . y axis compressed by factor of 27. Arrow scale is the same as in Fig. 13.

**Fig. 15** Simulated zeta potential for different models and electrolyte concentrations. DGML: model according to (2). Dilute: dilute solution model (3).

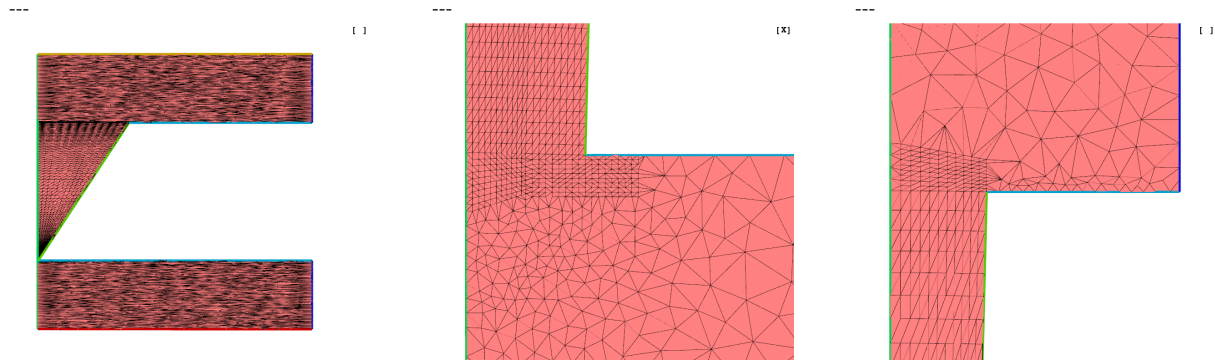
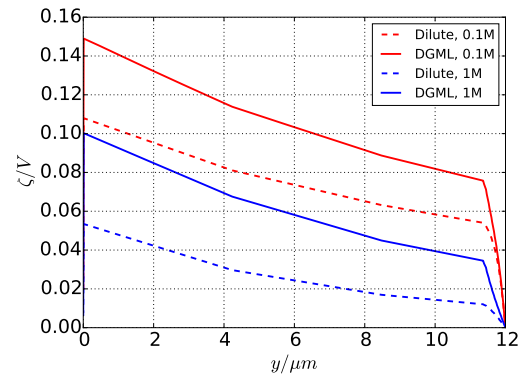
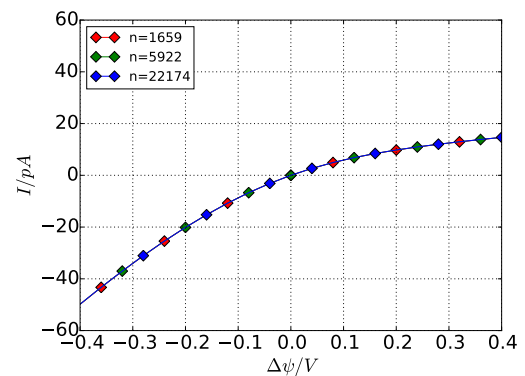


**Fig. 16** Left: full view of discretization grid,  $y$  axis compressed by factor of 27. Middle: detail at small opening. Right: detail at wide opening. The boundary layer at the pore wall is resolved by a fine grid along the whole pore.

**Fig. 17** IV-curve for electrolyte concentration  $0.1 \text{ mol/dm}^3$  with solvation effect on three subsequent grids



prediction. In order to maintain mass conservation, a high velocity at the wall need to be compensated by a flow in inverse direction in the center of the pore.

Calculations have been performed on a tailored boundary conforming Delaunay grid [SGF10] consisting of 5922 discretization nodes. It has been combined from a tapered, topologically rectangular grid for the inner part of the pore, from a rectangular grid in a boundary layer of width  $1.5 \text{ nm}$ , and from triangular grids for the lower and upper reservoir regions created using Triangle [She] with a number of a priori given grid points. Fig. 16 exhibits some features of this grid. Notable is the resolution of the polarization boundary layer with strongly anisotropic elements. Even on coarser grids, if they are well tailored, the presented method allows to obtain qualitatively meaningful results. Fig. 17 demonstrates the results for the calculation of the IV curve on three subsequent grids.

## 5 Conclusions

In this contribution, first results on a novel approach to the numerical solution of the Nernst-Planck-Poisson-Navier-Stokes system have been presented. The underlying model is based on first principles of nonequilibrium thermodynamics and includes ion-solvent interaction and solvation effects.

The discretization methods used are designed to preserve qualitative physical properties of the continuous model independent of the mesh size like mass conservation, pressure robustness, consistency to the thermodynamic equilibrium and maximum principle. A number of directions for future work arise:

- Investigation and improvement of the fixed point coupled solution approach.
- Incorporation of non-constant density into the pressure robust mixed finite element approach.
- Automatization of boundary layer adapted mesh generation for the finite volume method for general geometries in two and three space dimensions.
- Investigation of the existence and convergence of discrete solutions.
- Applications in nanofluidics, cell biology and other fields.

## References

- [AZJ<sup>+</sup>10] Y. Ai, M. Zhang, S.W. Joo, M.A. Cheney, and Sh. Qian. Effects of electroosmotic flow on ionic current rectification in conical nanopores. *J. Physical Chemistry C*, 114(9):3883–3890, 2010.
- [BB14] P. Berg and BE Benjaminsen. Effects of finite-size ions and relative permittivity in a nanopore model of a polymer electrolyte membrane. *Electrochimica Acta*, 120:429–438, 2014.
- [BF11] P. Berg and J. Findlay. Analytical solution of the Poisson–Nernst–Planck–Stokes equations in a cylindrical channel. *Proc. R. Soc. A*, 467(2135):3157–3169, 2011.
- [BFS14] D. Bothe, A. Fischer, and J. Saal. Global well-posedness and stability of electrokinetic flows. *SIAM J. Math. Anal.*, 46(2):1263–1316, 2014.
- [Bik42] J. J. Bikerman. Structure and capacity of electrical double layer. *Philos. Mag.*, 33(220):384–397, 1942.
- [BN64] D. Burgreen and F.R. Nakache. Electrokinetic flow in ultrafine capillary slits. *The Journal of Physical Chemistry*, 68(5):1084–1091, 1964.
- [BR85] Ch. Bernardi and G. Raugel. Analysis of some finite elements for the Stokes problem. *Math. Comp.*, 44(169):71–79, 1985.
- [BRF83] R.E. Bank, D.J. Rose, and W. Fichtner. Numerical methods for semiconductor device simulation. *SIAM J. Sci. Stat. Computing*, 4(3):416–435, 1983.
- [CDS12] H.C. Chang, E.A. Demekhin, and V.S. Shelistov. Competition between Dukhin’s and Rubinstein’s electrokinetic modes. *Phys. Rev. E*, 86(4):046319, 2012.
- [CI18] P. Constantin and M. Ignatova. On the Nernst-Planck-Navier-Stokes system. *arXiv:1806.11400*, 2018.
- [CS69] N. F. Carnahan and K. E. Starling. Equation of state for nonattracting rigid spheres. *J. Chem. Phys.*, 51:635, 1969.
- [DAM13] C.L. Druzgalski, M.B. Andersen, and A. Mani. Direct numerical simulation of electroconvective instability and hydrodynamic chaos near an ion-selective surface. *Physics of Fluids*, 25(11):110804, 2013.
- [DDGG17a] W. Dreyer, P. E. Druet, P. Gajewski, and C. Gohlke. Analysis of improved Nernst–Planck–Poisson models of compressible isothermal electrolytes. Part I: Derivation of the model and survey of the results, 2017. WIAS Berlin, preprint 2395.
- [DDGG17b] W. Dreyer, P. E. Druet, P. Gajewski, and C. Gohlke. Analysis of improved Nernst–Planck–Poisson models of compressible isothermal electrolytes. Part II: Approximation and a priori estimates, 2017. WIAS Berlin, preprint 2396.
- [DDGG17c] W. Dreyer, P. E. Druet, P. Gajewski, and C. Gohlke. Analysis of improved Nernst–Planck–Poisson models of compressible isothermal electrolytes. Part III: Compactness and convergence, 2017. WIAS Berlin, preprint 2397.
- [DGL14] W. Dreyer, C. Gohlke, and M. Landstorfer. A mixture theory of electrolytes containing solvation effects. *Electrochemistry Communications*, 43:75–78, 2014.
- [DGLM17] W. Dreyer, C. Gohlke, M. Landstorfer, and R. Müller. New insights on the interfacial tension of electrochemical interfaces and the Lippmann equation. *European J. Appl. Math.*, pages 1–46, 2017.
- [dGM62] S. R. de Groot and P. O. Mazur. *Non-Equilibrium Thermodynamics*. Dover Publications, 1962.
- [DGM13] W. Dreyer, C. Gohlke, and R. Müller. Overcoming the shortcomings of the Nernst–Planck model. *PCCP*, 15(19):7075–7086, 2013.
- [DOS05] H. Daiguji, Y. Oka, and K. Shirono. Nanofluidic diode and bipolar transistor. *Nano Letters*, 5(11):2274–2280, 2005.
- [DSP11] E.A. Demekhin, V.S. Shelistov, and S.V. Polyanskikh. Linear and nonlinear evolution and diffusion layer selection in electrokinetic instability. *Phys. Rev. E*, 84(3):036318, 2011.
- [Duk74] B.V. Dukhin, S.S. and Deryagin. *Surface and Colloid Science: Electrokinetic Phenomena*. Plenum Press, 1974.
- [DZR<sup>+</sup>11] E.V. Dydek, B. Zaltzman, I. Rubinstein, D.S. Deng, A. Mani, and M.Z. Bazant. Overlimiting current in a microchannel. *Phys. Rev. Letters*, 107(11):118301, 2011.
- [EFG06] R. Eymard, J. Fuhrmann, and K. Gärtner. A finite volume scheme for nonlinear parabolic equations derived from one-dimensional local Dirichlet problems. *Numer. Math.*, 102(3):463–495, 2006.
- [EGH00] R. Eymard, Th. Gallouët, and R. Herbin. Finite volume methods. *Handbook of numerical analysis*, 7:713–1018, 2000.
- [FLL11] J. Fuhrmann, A. Linke, and H. Langmach. A numerical method for mass conservative coupling between fluid flow and solute transport. *Applied Num. Math.*, 61(4):530–553, 2011.

- [FRD<sup>+</sup>17] P. Farrell, N. Rotundo, D.H. Doan, M. Kantner, J. Fuhrmann, and Th. Koprucki. Numerical methods for drift-diffusion models. In J. Piprek, editor, *Handbook of Optoelectronic Device Modeling and Simulation: Lasers, Modulators, Photodetectors, Solar Cells, and Numerical Methods*, volume 2, chapter 50, pages 733–771. CRC Press, Boca Raton, 2017.
- [Fre52] V. Freise. Zur Theorie der diffusen Doppelschicht. *Z. Elektrochem*, 56:822–827, 1952.
- [FRK11] F. Frank, N. Ray, and P. Knabner. Numerical investigation of homogenized Stokes–Nernst–Planck–Poisson systems. *Comp. and Vis. in Sci.*, 14(8):385–400, 2011.
- [FS17] André Fischer and Jürgen Saal. Global weak solutions in three space dimensions for electrokinetic flow processes. *Journal of Evolution Equations*, 17(1):309–333, 2017.
- [Fuh15] J. Fuhrmann. Comparison and numerical treatment of generalised Nernst–Planck models. *Computer Physics Comm.*, 196:166–178, 2015.
- [Fuh16] J. Fuhrmann. A numerical strategy for Nernst–Planck systems with solvation effect. *Fuel cells*, 16(6):704–714, 2016.
- [GR12] V. Girault and P.-A. Raviart. *Finite element methods for Navier–Stokes equations: theory and algorithms*, volume 5. Springer, 2012.
- [HS18] M. He and P. Sun. Mixed finite element analysis for the Poisson–Nernst–Planck/Stokes coupling. *J. Comp. and Appl. Math.*, 341:61–79, 2018.
- [Hun13] R. J. Hunter. *Zeta potential in colloid science: principles and applications*, volume 2. Academic press, 2013.
- [Il<sup>69</sup>] A. M. Il’in. A difference scheme for a differential equation with a small parameter multiplying the second derivative. *Mat. zametki*, 6:237–248, 1969.
- [Jer02] J. W. Jerome. Analytical approaches to charge transport in a moving medium. *Transport Theory and Stat. Phys.*, 31(4-6):333–366, 2002.
- [JF<sup>+</sup>18] T. Streckenbach J. Fuhrmann et al. pdelib. <http://pdelib.org>, 2018.
- [JLM<sup>+</sup>17] V. John, A. Linke, C. Merdon, M. Neilan, and L. G. Rebholz. On the divergence constraint in mixed finite element methods for incompressible flows. *SIAM Review*, 59(3):492–544, 2017.
- [Joh16] V. John. *Finite element methods for incompressible flow problems*. Springer, 2016.
- [Jün15] A. Jüngel. The boundedness-by-entropy method for cross-diffusion systems. *Nonlinearity*, 28(6):1963, 2015.
- [KBA07] M. S. Kiliç, M. Z. Bazant, and A. Ajdari. Steric effects in the dynamics of electrolytes at large applied voltages. i. double-layer charging. *Phys. Rev. E*, 75(2):021502, 2007.
- [KDM15] E. Karatay, C. L. Druzgalski, and A. Mani. Simulation of chaotic electrokinetic transport: Performance of commercial software versus custom-built direct numerical simulation codes. *J. Colloid Interface Sci.*, 446:67–76, 2015.
- [KFND10] F. Keller, M. Feist, H. Nirschl, and W. Dörfler. Investigation of the nonlinear effects during the sedimentation process of a charged colloidal particle by direct numerical simulation. *J. Colloid and Interface Sci.*, 344(1):228–236, 2010.
- [KV81] A. A. Kornyshev and M. A. Vorotyntsev. Conductivity and space charge phenomena in solid electrolytes with one mobile charge carrier species, a review with original material. *Electrochim. Acta*, 26(3):303–323, 1981.
- [LFY02] J.Y. Lin, L.M. Fu, and R.J. Yang. Numerical simulation of electrokinetic focusing in microfluidic chips. *J. Micromech. and Microengr.*, 12(6):955, 2002.
- [LGD16] M. Landstorfer, C. Gohlke, and W. Dreyer. Theory and structure of the metal-electrolyte interface incorporating adsorption and solvation effects. *Electrochimica Acta*, 201:187–219, 2016.
- [Lin14] A. Linke. On the role of the Helmholtz decomposition in mixed methods for incompressible flows and a new variational crime. *Computer methods in applied mechanics and engineering*, 268:782–800, 2014.
- [LM16] A. Linke and Ch. Merdon. Pressure-robustness and discrete Helmholtz projectors in mixed finite element methods for the incompressible Navier–Stokes equations. *CMAME*, 311:304–326, 2016.
- [LMV96] R. D. Lazarov, I.D. Mishev, and P. S. Vassilevski. Finite volume methods for convection-diffusion problems. *SIAM J. Numer. Anal.*, 33(1):31–55, 1996.
- [Lyk05] J. Lyklema. *Fundamentals of interface and colloid science: soft colloids*, volume 5. Elsevier, 2005.
- [MCSJ71] G. A. Mansoori, N. F. Carnahan, K. E. Starling, and T. W. Leland Jr. Equilibrium thermodynamic properties of the mixture of hard spheres. *J. Chem. Phys.*, 54:1523, 1971.
- [MFL<sup>+</sup>16] C. Merdon, J. Fuhrmann, A. Linke, T. Streckenbach, F. Neumann, M. Khodayari, and H. Baltruschat. Inverse modeling of thin layer flow cells for detection of solubility, transport and reaction coefficients from experimental data. *Electrochimica Acta*, 211:1–10, 2016.
- [MW94] J. J. H. Miller and S. Wang. An analysis of the Scharfetter–Gummel box method for the stationary semiconductor device equations. *RAIRO-Modélisation mathématique et analyse numérique*, 28(2):123–140, 1994.
- [Ner88] W. Nernst. Zur Kinetik der in Lösung befindlichen Körper. *Z. phys. Chemie*, 2(1):613–637, 1888.
- [NKU<sup>+</sup>14] V.V. Nikonenko, A.V. Kovalenko, M. K. Urtenov, N.D. Pismenskaya, J. Han, Ph. Sistat, and G. Pourcelly. Desalination at overlimiting currents: State-of-the-art and perspectives. *Desalination*, 342:85–106, 2014.
- [Ove52] J.Th. Overbeek. Electrokinetic phenomena. In H. R. Kruyt, editor, *Colloid science*, volume 1, pages 194–244. Elsevier, Amsterdam, 1952.
- [Pla90] M. Planck. Über die Erregung von Electricität und Wärme in Electrolyten. *Annalen der Physik*, 275(2):161–186, 1890.
- [PLL<sup>+</sup>12] V. S. Pham, Z. Li, K. M. Lim, J. K. White, and J. Han. Direct numerical simulation of electroconvective instability and hysteretic current-voltage response of a permselective membrane. *Phys. I Rev. E*, 86(4):046310, 2012.
- [PS10] A. Prohl and M. Schmuck. Convergent finite element discretizations of the Navier–Stokes–Nernst–Planck–Poisson system. *ESAIM: Math. Modelling and Num. Analysis*, 44(3):531–571, 2010.
- [PSD<sup>+</sup>11] M.R. Powell, N. Sa, M. Davenport, K. Healy, I. Vlassioux, S.E. Letant, L.A. Baker, and Z.S. Siwy. Noise properties of rectifying nanopores. *J. Phys. Chem. C*, 115(17):8775–8783, 2011.
- [RDHdG16] G. Rempfer, G. B. Davies, Ch. Holm, and J. de Graaf. Reducing spurious flow in simulations of electrokinetic phenomena. *J. Chem. Physics*, 145(4):044901, 2016.
- [RM17] I. I. Ryzhkov and A.V. Minakov. Finite ion size effects on electrolyte transport in nanofiltration membranes. *J. Sib. Fed. Univ. Mathematics & Physics*, 10(2):186, 2017.
- [Ryh06] R.J. Ryham. *An energetic variational approach to mathematical modeling of charged fluids: charge phases, simulation and well posedness*. PhD thesis, Pennsylvania State Univ., 2006.
- [Ryh09] R. J. Ryham. Existence, uniqueness, regularity and long-term behavior for dissipative systems modeling electrohydrodynamics. *arXiv preprint arXiv:0910.4973*, 2009.

- [RZ00] I. Rubinstein and B. Zaltzman. Electro-osmotically induced convection at a permselective membrane. *Phys. Rev. E*, 62(2):2238, 2000.
- [SAMJ17] R. Sacco, P. Airoldi, A.G. Mauri, and J.W. Jerome. Three-dimensional simulation of biological ion channels under mechanical, thermal and fluid forces. *Applied Mathematical Modelling*, 43:221–251, 2017.
- [Sch09] M. Schmuck. Analysis of the Navier–Stokes–Nernst–Planck–Poisson system. *Math. Models and Methods in App. Sci.*, 19(06):993–1014, 2009.
- [SF02] Z. Siwy and A. Fuliński. Fabrication of a synthetic nanopore ion pump. *Phys. Rev. Letters*, 89(19):198103, 2002.
- [SG69] D.L. Scharfetter and H.K. Gummel. Large-signal analysis of a silicon Read diode oscillator. *IEEE Trans. Electron. Dev.*, 16(1):64–77, 1969.
- [SG04] O. Schenk and K. Gärtner. Solving unsymmetric sparse systems of linear equations with PARDISO. *Future Generation Computer Systems*, 20(3):475–487, 2004.
- [SG<sup>+</sup>17] O. Schenk, K. Gärtner, et al. PARDISO Solver Project. URL: <http://www.pardiso-project.org>, 2017. Accessed 2017-01-01.
- [SGF10] H. Si, K. Gärtner, and J. Fuhrmann. Boundary conforming Delaunay mesh generation. *Comput. Math. Math. Phys.*, 50:38–53, 2010.
- [SGS<sup>+</sup>02] Z. Siwy, Y. Gu, H.A. Spohr, D. Baur, A. Wolf-Reber, R. Spohr, P. Apel, and Y.E. Korchev. Rectification and voltage gating of ion currents in a nanofabricated pore. *Europhysics Letters*, 60(3):349, 2002.
- [She] J. Shewchuk. Triangle: A two-dimensional quality mesh generator and Delaunay triangulator. URL: <http://www.cs.cmu.edu/~quake/triangle.html>. Accessed 2017-01-01.
- [Smo21] M von Smoluchowski. Elektrische Endosmose und Strömungströme. In L. Graetz, editor, *Handbuch der Electricität und des Magnetismus Band II*, pages 366–427. Barth, Leipzig, 1921.
- [Ste24] O. Stern. Zur Theorie der elektrolytischen Doppelschicht. *Z. f. Electrochemie*, 30:508, 1924.
- [TYCG03] G.Y. Tang, C. Yang, C.J. Chai, and H.Q. Gong. Modeling of electroosmotic flow and capillary electrophoresis with the joule heating effect: The Nernst-Planck equation versus the Boltzmann distribution. *Langmuir*, 19(26):10975–10984, 2003.
- [WBPS17] Ch. Wang, J. Bao, W. Pan, and X. Sun. Modeling electrokinetics in ionic liquids. *Electrophoresis*, 38(13-14):1693–1705, 2017.
- [WBS10] M.T. Wolfram, M. Burger, and Z.S. Siwy. Mathematical modeling and simulation of nanopore blocking by precipitation. *J. Physics: Condensed Matter*, 22(45):454101, 2010.
- [WPC<sup>+</sup>09] Y. Wang, K. Pant, Zh. Chen, G. Wang, W. F. Diffey, P. Ashley, and Sh. Sundaram. Numerical analysis of electrokinetic transport in micro-nanofluidic interconnect preconcentrator in hydrodynamic flow. *Microfluidics and nanofluidics*, 7(5):683, 2009.
- [XZ99] J. Xu and L. Zikatanov. A monotone finite element scheme for convection-diffusion equations. *Math. Comp.*, 68(228):1429–1446, 1999.